NUCL SCI TECH (2019) 30:101
https://doi.org/10.1007/s41365-019-0612-4

Transfer function measurement for the SSRF SRF system

Yang-Yang Xia[1,2] · **Zhen-Tang Zhao**[1] · **Yu-Bin Zhao**[1] · **Xiang Zheng**[1] ·
Kai Xu[1] · **Zhi-Gang Zhang**[1] · **Shen-Jie Zhao**[1] · **Qiang Chang**[1]

Received: 30 October 2018 / Revised: 19 February 2019 / Accepted: 23 February 2019 /

Abstract A digital transfer function measurement system has been embedded in the low-level radio frequency (LLRF) system of the storage ring of the Shanghai Synchrotron Radiation Facility. The measurement results indicate that the decreased control accuracy at high current is primarily owing to ripples from the high-voltage power supply, the transient beam loading effect, and the digital aliasing effect. The current LLRF algorithm is not able to suppress these disturbances.

Keywords Transfer function · Ripples of HVPS · Transient beam loading effect

1 Introduction

Since 2008, three superconducting cavities [1, 2] have been installed in the storage ring of the Shanghai Synchrotron Radiation Facility (SSRF) to provide beam accelerating voltage and RF power for generating synchrotron radiation. Currently, the SRF system of the SSRF is suffering from two problems. One is the low beam current limit, which is significantly smaller than that predicted by the Robinson criterion. The other is the disturbed radiation luminous flux; it has been confirmed that the disturbance signal comes from the heavily beam-loaded SRF system. The first problem seems to be a "Robinson-like" instability issue and can be resolved by increasing the accelerating voltage or decreasing the beam loading phase. However, a sudden voltage drop, which is considered to result from the multipacting effect, occurs frequently during high-voltage operation [3]. A direct feedback loop was added to the low-level radio frequency (LLRF) system, and the beam current limit indeed increased [4–7]. The beam current limit can be increased from 140 to 220 mA when the total accelerating voltage is 3.3 MV, and the equivalent direct feedback gain is 0.4. However, this result is still much lower than expected. According to the modified Robinson criterion with direct feedback, the beam current limit should be 298 mA when the beam loading phase is − 10°. The second problem is a disturbance rejection issue. The current LLRF system [8–12] at SSRF is not able to suppress the disturbance signal when beam loading is heavy. The low-frequency power disturbance signal, high-voltage power supply (HVPS) PWM interference signal, transient beam loading noise, and its digital aliasing signal are the main sources of disturbance. Infrared luminous flux measurement from the beamline station indicates that the disturbance signal is amplified as the beam increases.

Solutions to these two problems can be found in loop design, and the interaction between the control system and RF system is commonly simulated by the Pedersen model [13–16]. However, the system is quite complicated when a digital control algorithm is considered, and the multiple control units (three RF stations) make the whole system much more complex.

In this paper, a digital transfer function measurement system embedded into the LLRF system is introduced to measure the transfer function and system performance with various operation statuses. The measurement principles and results will also be discussed in the following sections.

✉ Zhen-Tang Zhao
zhaozhentang@sinap.ac.cn

[1] Shanghai Institute of Applied Physics, Chinese Academy of Sciences, Shanghai 201800, China

[2] University of Chinese Academy of Sciences, Beijing 100049, China

2 SRF system and transfer function measurement system

2.1 SRF system

The RF power supply of the SSRF storage ring is in a distributed style, which means that one RF station only controls one superconducting cavity. A solid-state amplifier and klystron realize two-stage power amplification, and cavity resonance is tuned by a stepper motor. All the control signals are provided by the LLRF system. The basic parameters of the SRF system are listed in Table 1.

The entire LLRF system consists of four classical feedback loops: an amplitude loop, phase loop, tuning loop, and direct feedback loop [17]. The amplitude and phase loops together are considered the field loop. The main hardware algorithm diagram is shown in Fig. 1.

The 500-MHz RF signal from the cavity probe is down-converted to a 31.25-MHz intermediate frequency (IF) signal and then transformed into a digital data flow by an analog–digital converter (ADC). The baseband in-phase and quadrature (IQ) components are then extracted from the data flow using a digital IQ demodulation module. If the IF signal is a pure cosine wave, the arithmetic expressions of the in-phase (I) and quadrature components (Q) are:

$$\begin{aligned} y(t) &= A\cos(\omega t + \varphi_0) \\ &= A\cos\varphi_0\cos(\omega t) - A\sin\varphi_0\sin(\omega t) \\ I(t) &= A\cos\varphi_0 \\ Q(t) &= A\sin\varphi_0 \end{aligned}, \qquad (1)$$

where A, φ_0, and ω are the amplitude, initial phase, and frequency of the wave, respectively.

The cavity voltage IQ components ($I_{\text{cavity\_voltage}}/Q_{\text{cavity\_voltage}}$) are first calibrated by a rotation module to compensate for the—phase mismatching and gain mismatching in the feedback path. IQ errors are calculated by subtracting the calibrated cavity voltage IQ component from the reference IQ values. The IQ errors are fed into two proportional–integral (PI) controllers. If the direct feedback loop is closed, the cavity voltage IQ components are phase-shifted and amplified by another rotation module and then subtracted by the processed data from the PI controllers to obtain the main control data. The direct feedback loop is in addition to the digital feedback loop acting on the RF field. If the transfer function measurement system is operating, the main control data combines the disturbance signal ($I_{\text{disturbance}}/Q_{\text{disturbance}}$) with the real control data ($I_{\text{output}}/Q_{\text{output}}$). A digital IQ modulation module produces the IF digital data flow from the real control data, and the digital–analog converter (DAC) transforms the data flow into an analog signal whose carrier

Table 1 Basic parameters of the SRF system

Parameters	Value
Central frequency, f_c (MHz)	499.683
Geometric structure factor, ${}^{r}/_{Q}$ (Ω)	89
Loaded quality factor, Q_L	$\sim 1.7 \times 10^5$

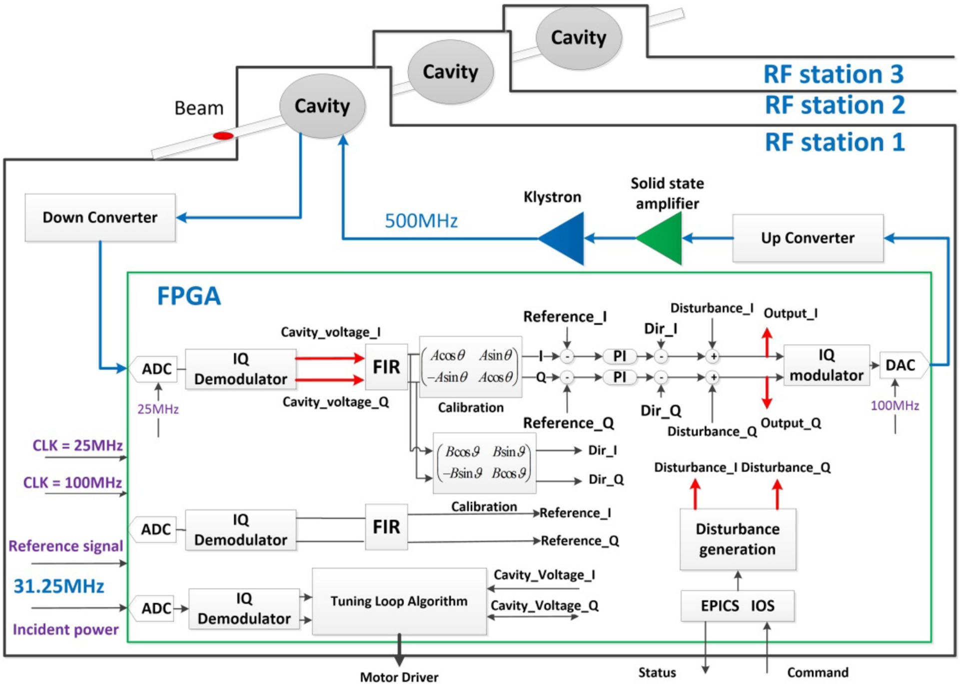

Fig. 1 SRF system diagram in the SSRF storage ring. The red arrows denote nodes in the data flow recorded by the transfer function measurement system

frequency is 31.25 MHz. The output analog signal from the LLRF digital data processing (DSP) board is up-converted to a 500-MHz RF signal and fed into the two-stage amplification power system (solid-state amplifier and klystron) to close the main feedback loop [18].

2.2 Principle of transfer function measurement

The process of transfer function measurement is programmed and embedded into the field programmable gate array (FPGA) of the DSP board. First, the disturbance signal generation module receives the modulation information (ω_k, D_k) from the master controller and produces IQ data flows of the disturbance signal. Second, the disturbance data flows ($I_{\text{disturbance}}/Q_{\text{disturbance}}$) are added to the main loop path to realize the disturbance addition. Third, the recording module starts recording data from three nodes ($I_{\text{cavity\_voltage}}/Q_{\text{cavity\_voltage}}, I_{\text{output}}/Q_{\text{output}}, I_{\text{disturbance}}/Q_{\text{disturbance}}$) after a 1-ms time delay from step 2 to ensure that the field established in the cavity is stable. Fourth, the recorded data are uploaded to the master controller, and one measurement cycle is finished. The whole process consists of 3000 measurement cycles, and a 10-Hz step in frequency is the only difference between adjacent cycles. The scanning frequency range is from 10 Hz to 30 kHz. The transfer function for specific operation conditions is extracted from the measured data flow.

The IQ components of the disturbance signal can be expressed as:

$$\begin{aligned} I[n] &= D_k\cos(\omega_k n + \varphi_{k\text{d}}) \\ Q[n] &= 0 \end{aligned}, \tag{2}$$

where ω_k, $\varphi_{k\text{d}}$, and D_k are the frequency, initial phase, and magnitude of the kth disturbance signal, respectively, as applied in one transfer function measurement cycle; and n is the sampling number.

The initial phase (φ_{0k}) of the real control data is the phase angle of ($I_{\text{output\_DC}} + jQ_{\text{output\_DC}}$), where $I_{\text{output\_DC}}$ and $Q_{\text{output\_DC}}$ are direct components of the real control data, and j is the imaginary number, which satisfies $\sqrt{-1} = \pm j$.

The disturbed IQ components of the cavity voltage can be expressed as:

$$\begin{aligned} I[n] &= I_{\text{DC}} + a_k\cos(\omega_k n + \varphi_{k\text{a}}) \\ &\quad \times I_{\text{DC}} + p_k\cos(\omega_k n + \varphi_{k\text{p}}) \times Q_{\text{DC}} \\ Q[n] &= Q_{\text{DC}} + a_k\cos(\omega_k n + \varphi_{k\text{a}}) \\ &\quad \times Q_{\text{DC}} - p_k\cos(\omega_k n + \varphi_{k\text{p}}) \times I_{\text{DC}} \end{aligned}, \tag{3}$$

where $\varphi_{k\text{a}}/\varphi_{k\text{p}}$ is the initial phase of the amplitude modulation (AM)/phase modulation (PM) signal for the kth measurement cycle, a_k/p_k is the relative amplitude of the AM/PM, and $I_{\text{DC}}/Q_{\text{DC}}$ is the direct component of the in-phase/quadrature component. Typical IQ data flows for various nodes are shown in Fig. 2.

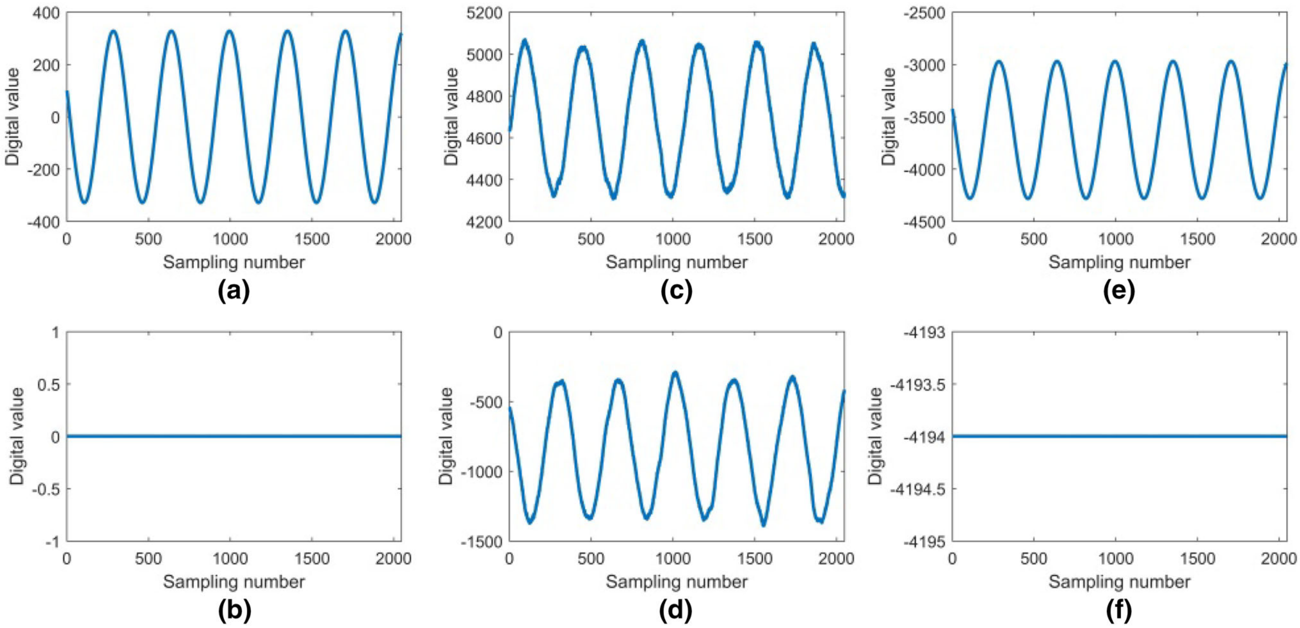

Fig. 2 Typical IQ data flows for various nodes when disturbance is added: **a** in-phase component of disturbance signal; **b** quadrature component of disturbance signal; **c** in-phase component of cavity voltage; **d** quadrature component of cavity voltage; **e** in-phase component of digital output; **f** quadrature component of digital output. The disturbance frequency is 1.1 kHz, and the sampling frequency is 390.625 kHz

The polar expressions of the cavity voltage are:

$$A[n]=\sqrt{I[n]^2+Q[n]^2}$$
$$P[n]=\begin{cases}\arctan\left(\dfrac{Q[n]}{I[n]}\right) & I[n]>0\\ +\dfrac{\pi}{2} & I[n]=0, Q[n]>0\\ -\dfrac{\pi}{2} & I[n]=0, Q[n]<0\\ \operatorname{sign}(Q[n])\times\pi+\arctan\left(\dfrac{Q[n]}{I[n]}\right) & I[n]<0\end{cases}, \tag{4}$$

where $A[n]$ and $P[n]$ represent the amplitude and phase of the cavity voltage data flow, respectively.

The amplitude modulation information and phase modulation information can be derived from the amplitude and phase of the data flow by fitting with

$$y[n]=y_{0k}+y_{1k}\cos\left(2\pi\frac{f_k}{f_\mathrm{s}}n+\varphi_k\right), \tag{5}$$

where y_{0k} is the direct component of the fitted data flow, y_{1k} is the modulation amplitude, f_k is the modulation frequency, f_s is the sampling frequency, and φ_k is the modulation initial phase.

The relative amplitude of AM/PM is considered small compared with the signal DC components. By substituting Eq. (3) into Eq. (4) and ignoring the high-order minima, except for the first-order minima, the polar expressions of the cavity voltage can be written as:

By comparing with Eqs. (3) and (6), the congruent relationship is

$$\begin{aligned} a_k &= \frac{y_{1k}}{y_{0k}} && (A[n]\text{ data flow})\\ p_k &= y_{1k} && (P[n]\text{ data flow})\\ \varphi_{0k} &= y_{0k} && (P[n]\text{ data flow})\\ \varphi_{ka} &= \varphi_k && (A[n]\text{ data flow})\\ \varphi_{kp} &= \varphi_k+\pi && (P[n]\text{ data flow})\\ \omega_k &= 2\pi\frac{f_k}{f_\mathrm{s}} \end{aligned}. \tag{7}$$

The frequency response $f_{\text{cavity\_voltage}}(\omega)$ of the cavity voltage is derived from Eq. (7) by

$$\Delta\varphi_\mathrm{a}=\varphi_{k\mathrm{a}}-\varphi_{0k},$$
$$\Delta\varphi_\mathrm{p}=\varphi_{k\mathrm{p}}-\varphi_{0k},$$
$$\begin{cases} f_{\text{cavity\_voltage}}(\omega_k)=\dfrac{1}{2}\left(a_k\mathrm{e}^{j\Delta\varphi_\mathrm{a}}+jp_k\mathrm{e}^{j\Delta\varphi_\mathrm{p}}\right)\\ f_{\text{cavity\_voltage}}(-\omega_k)=\dfrac{1}{2}\left(a_k\mathrm{e}^{-j\Delta\varphi_\mathrm{a}}+jp_k\mathrm{e}^{-j\Delta\varphi_\mathrm{p}}\right)\end{cases}.\quad(\omega_k>0) \tag{8}$$

The derivation of the closed-loop transfer function $T(\omega)$ (from incident power to cavity voltage) combines the information concerning the real control data and disturbance signal. The absolute value of the disturbance amplitude can be derived by fitting the in-phase (I) component of the disturbance signal with Eq. (5). The congruent relationship is given by:

$$\begin{aligned} A[n]&=\sqrt{I[n]^2+Q[n]^2}\\ &\approx\sqrt{I_\mathrm{DC}^2(1+2a_k\cos(\omega_kn+\varphi_{k\mathrm{a}}))+p_k\cos(\omega_kn+\varphi_{k\mathrm{p}})Q_\mathrm{DC}I_\mathrm{DC}+Q_\mathrm{DC}^2(1+2a_k\cos(\omega_kn+\varphi_{k\mathrm{a}}))-p_k\cos(\omega_kn+\varphi_{k\mathrm{p}})Q_\mathrm{DC}I_\mathrm{DC}}\\ &=\sqrt{(I_\mathrm{DC}^2+Q_\mathrm{DC}^2)(1+2a_k\cos(\omega_kn+\varphi_{k\mathrm{a}}))}\approx(1+a_k\cos(\omega_kn+\varphi_{k\mathrm{a}}))\sqrt{(I_\mathrm{DC}^2+Q_\mathrm{DC}^2)},\\ P[n]&=\arctan\left(\frac{Q[n]}{I[n]}\right)\\ &=\arctan\left(\frac{Q_\mathrm{DC}+a_k\cos(\omega_kn+\varphi_{k\mathrm{a}})\times Q_\mathrm{DC}-p_k\cos(\omega_kn+\varphi_{k\mathrm{p}})\times I_\mathrm{DC}}{I_\mathrm{DC}+a_k\cos(\omega_kn+\varphi_{k\mathrm{a}})\times I_\mathrm{DC}+p_k\cos(\omega_kn+\varphi_{k\mathrm{p}})\times Q_\mathrm{DC}}\right)\\ &=\arctan\left({}^{Q_\mathrm{DC}}\!/_{I_\mathrm{DC}}\left(1-\frac{p_k\cos(\omega_kn+\varphi_{k\mathrm{p}})\times Q_\mathrm{DC}/I_\mathrm{DC}+p_k\cos(\omega_kn+\varphi_{k\mathrm{p}})I_\mathrm{DC}/Q_\mathrm{DC}}{1+a_k\cos(\omega_kn+\varphi_{k\mathrm{a}})+p_k\cos(\omega_kn+\varphi_{k\mathrm{p}})\times {}^{Q_\mathrm{DC}}\!/_{I_\mathrm{DC}}}\right)\right)\\ &\approx\arctan\left({}^{Q_\mathrm{DC}}\!/_{I_\mathrm{DC}}\right)-\frac{p_k\cos(\omega_kn+\varphi_{k\mathrm{p}})}{1+a_k\cos(\omega_kn+\varphi_{k\mathrm{a}})+p_k\cos(\omega_kn+\varphi_{k\mathrm{p}})\times {}^{Q_\mathrm{DC}}\!/_{I_\mathrm{DC}}}\\ &\approx\arctan\left({}^{Q_\mathrm{DC}}\!/_{I_\mathrm{DC}}\right)-p_k\cos(\omega_kn+\varphi_{k\mathrm{p}}). \end{aligned} \tag{6}$$

$$
\begin{aligned}
D_k &= y_{1k},\\
y_{0k} &= 0,\\
\varphi_{kd} &= \phi_k.
\end{aligned}
\tag{9}
$$

The information regarding the equivalent AM and PM for the disturbance signal is given by:

$$
\begin{aligned}
a_k^E &= D_k \frac{\left|I_{\text{output\_DC}}\right|}{I^2_{\text{output\_DC}} + Q^2_{\text{output\_DC}}},\\
\varphi_{ka}^E &= \varphi_{kd} + \frac{\left(\operatorname{sign}\left(\left|I_{\text{output\_DC}}\right|\right) - 1\right)}{2}\pi,\\
p_k^E &= a_k^E \times \left|\frac{Q_{\text{output\_DC}}}{I_{\text{output\_DC}}}\right|,\\
\varphi_{kp}^E &= \varphi_{ka}^E + \frac{\left(\operatorname{sign}\left(-\frac{Q_{\text{output\_DC}}}{\left|I_{\text{output\_DC}}\right|}\right) - 1\right)}{2}\pi,\\
\varphi_{0k}^E &= \varphi_{0k} \quad \text{(the same value of the real control data)}
\end{aligned}
\tag{10}
$$

The $T(\omega)$ can be derived from

$$
\begin{aligned}
&\Delta\varphi_{\mathrm{a}}^E = \varphi_{ka}^E - \varphi_{0k}^E,\\
&\Delta\varphi_{\mathrm{p}}^E = \varphi_{kp}^E - \varphi_{0k}^E,\\
&\begin{cases}
f_{\text{disturbance}}(j\omega_k) = \frac{1}{2}\left(a_k^E \mathrm{e}^{j\Delta\varphi_{\mathrm{a}}^E} + jp_k^E \mathrm{e}^{j\Delta\varphi_{\mathrm{p}}^E}\right)\\
f_{\text{disturbance}}(-j\omega_k) = \frac{1}{2}\left(a_k^E \mathrm{e}^{-j\Delta\varphi_{\mathrm{a}}^E} + jp_k^E \mathrm{e}^{-j\Delta\varphi_{\mathrm{p}}^E}\right)
\end{cases} (\omega_k > 0),\\
&T(j\omega) = \frac{f_{\text{cavity\_voltage}}(j\omega)}{f_{\text{disturbance}}(j\omega)}
\end{aligned}
\tag{11}
$$

The superscript “E” denotes the parameters equivalent to those of the open-loop measurement.

The measurement system can also acquire the real-time control status by recording data without internal disturbance generation. These data can be used to analyze the real system performance with respect to various operation statuses.

3 Experiment results

3.1 SRF parameter regulation by open-loop transfer function measurement

The control model for the open-loop SRF system can be simplified to:

$$
\begin{aligned}
G_0(s) &= \frac{2\sigma R s}{s^2 + 2\sigma s + \omega_{\mathrm{r}}^2}\mathrm{e}^{-\tau s},\\
R &= \frac{1}{2}\frac{r}{Q}Q_{\mathrm{L}},\\
\sigma &= \frac{\omega_{\mathrm{r}}}{2Q_{\mathrm{L}}},
\end{aligned}
\tag{12}
$$

where $^r/_Q$ is the geometric structure factor of the superconducting cavity, Q_{L} is the loaded quality factor, and τ is the group delay time. Considering the measurements are realized in the baseband of the digital path (IQ component), there is a frequency shift on Eq. (12) [19]. The practical control model is:

$$
G(s) = \frac{G_0(s + j\omega_{\mathrm{c}})}{G_0(j\omega_{\mathrm{c}})},
\tag{13}
$$

where ω_{c} is the carrier frequency of the RF analog signal.

The loaded quality factor, SRF resonance frequency, and group delay time can be derived from the phase–frequency response curve by fitting with Eq. (13). The fitted results are listed in Table 2. Δf denotes the frequency difference between central frequency and resonance frequency, and the resonance frequency is smaller than central frequency when Δf is less than zero. The value of the loaded quality factor seen by the LLRF system is 11% less than that provided by the cavity manufacturer.

A comparison of the simulated and experimental frequency responses is shown in Fig. 3.

3.2 Closed-loop transfer function

The transfer functions with the loop closed are quite different from those obtained with the loop open. The closed-loop transfer function is strongly related to the choice of control parameters and operation conditions of the RF station. The amplitude–frequency responses with various control parameters when there is no beam in the storage ring and the cavity is tuned near resonance are shown in Fig. 4.

It is concluded that as the proportional term of the PI controller (kp) increases, the gain of the transfer function decreases; in addition, as the integral term of the PI

Table 2 Regulated SRF parameters

Parameters	Value
ω_{r} (MHz)	$2\pi \times 499.683$
Δf (Hz)	-2699
Q_{L}	1.5×10^5
τ (μs)	1.36

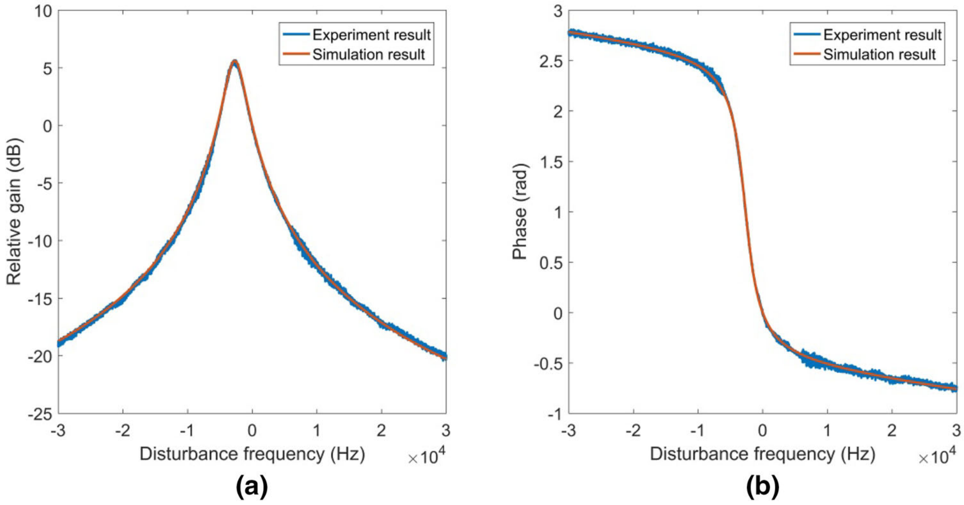

Fig. 3 Comparison of simulated and experimental frequency responses: **a** amplitude–frequency response; **b** phase–frequency response (Color online)

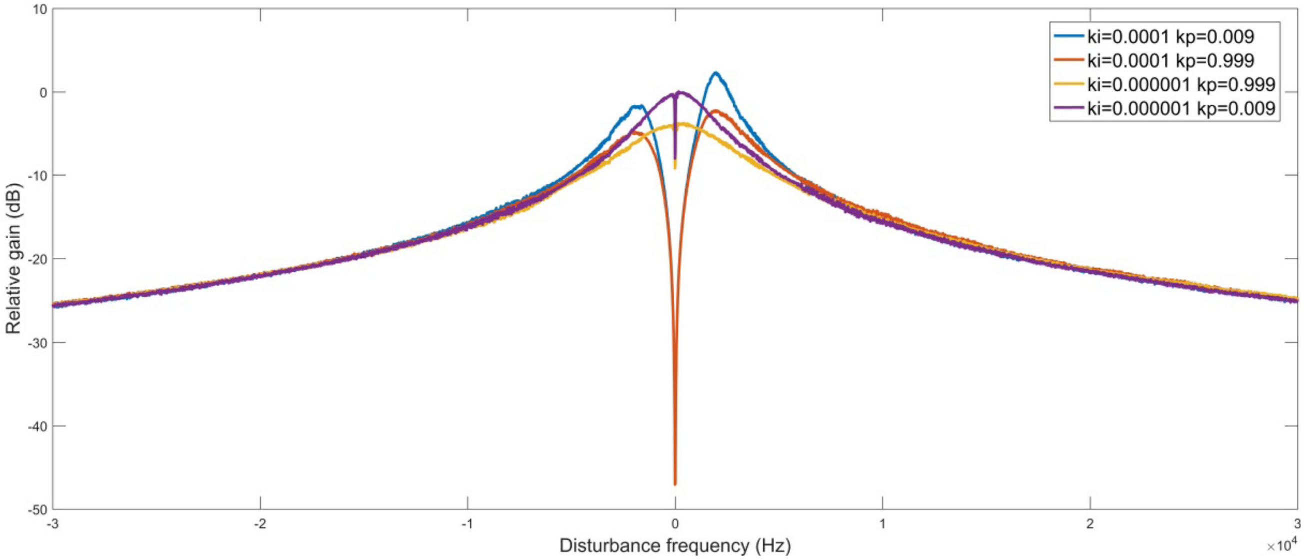

Fig. 4 Closed-loop transfer functions under various operation conditions without beam current. The cavity is tuned near resonance

controller (ki) decreases, the maximum gain of the transfer function also decreases. However, the decreasing integral term of the PI controller can increase the gain of the transfer function near the carrier frequency.

During transfer function measurement with a beam, one cavity is far detuned and the accelerating voltage for the other two cavities is 1.2 MV. The set value of the beam loading phase for both RF stations is near 0°. The synchronous phase difference between two RF stations is approximately 22°. RF station 1 offers more power to the beam. The parameters of the PI controller for both RF stations are fixed during beam injection. The operation statuses for the two RF stations during measurement are listed in Table 3. Measurements were performed at RF station 1. DRFB is an acronym for direct feedback, and the gain was set at 0.5. The number after every control parameter denotes the index of the RF station controller they were set in.

The amplitude–frequency responses under various operation conditions are shown in Fig. 5.

As the beam current increases, the transfer function is seriously distorted. The maximum gain of the transfer function is increased, and the result is related to the control status of RF station 2. The influence of other stations means that interaction between stations is not negligible. The rules regarding the impact on transfer function distortion with various parameter choices, which are derived from measurement without the beam, still apply here.

Table 3 Operation statuses during measurements

	ki1	kp1	ki2	kp2	DRFB1	DRFB2	Current (mA)
Case 1	0.0001	0.009	0.000001	0.999	Off	Off	0
Case 2	0.0001	0.009	0.000001	0.999	Off	Off	100
Case 3	0.0001	0.009	0.000001	0.999	Off	On	100
Case 4	0.000001	0.999	0.000001	0.999	On	Off	100

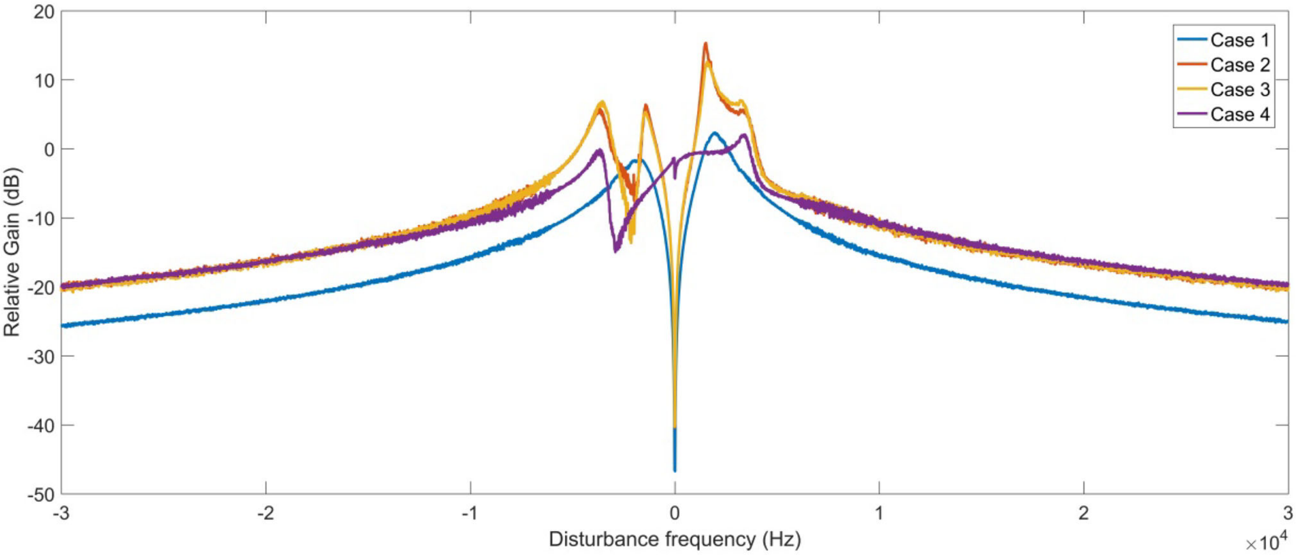

Fig. 5 Transfer functions under various operation statuses. Transfer function with the beam is seriously distorted from that without the beam. The control parameters of case 2 and case 3 will amplify the modulation signal, whose frequency ranges from + 800 to + 4500 Hz. The transfer function difference between case 2 and case 3 indicates the existence of interaction between RF stations (Color online)

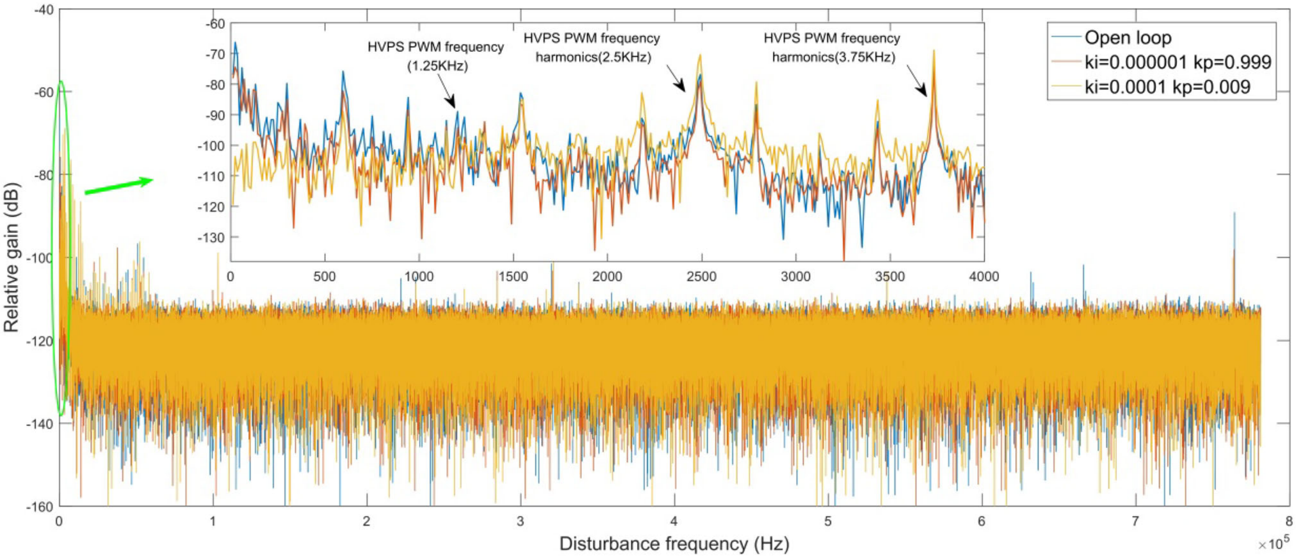

Fig. 6 Spectra of the disturbance signal under various control conditions without the beam. The frequency of the disturbance signal, when no beam is in the storage ring, is centered near the carrier frequency. The closed loop rejects the disturbance signal in some frequency range and amplifies it in some other frequency range. The gain of the amplification is strongly related to the choice of control parameters (Color online)

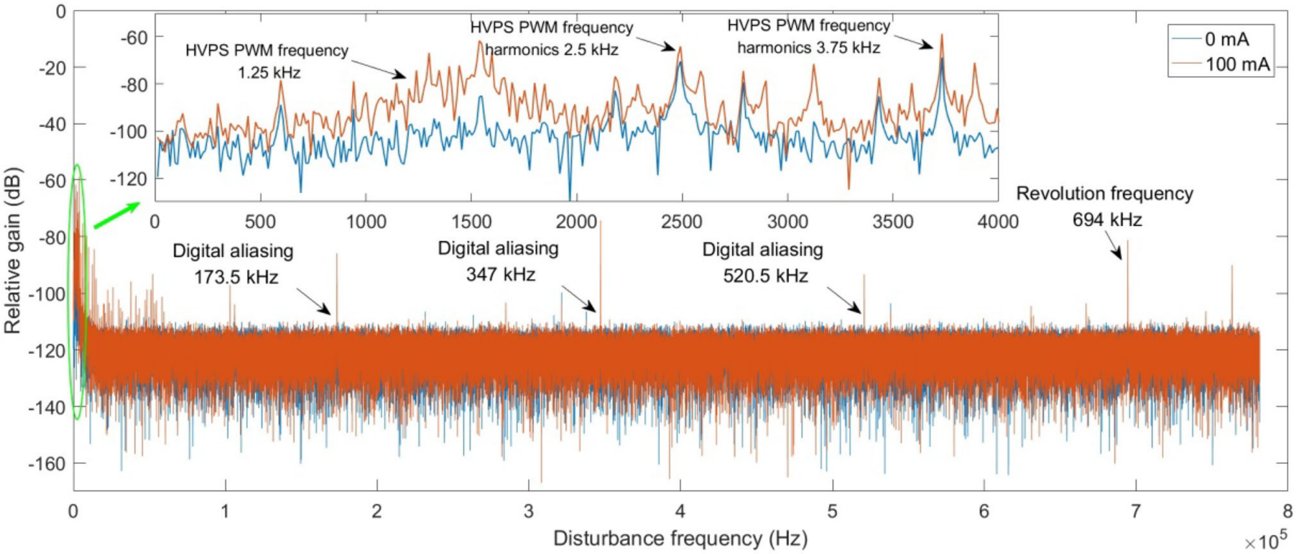

Fig. 7 Spectra of the disturbance signal under various control conditions with the beam. The control status (ki = 0.0001 kp = 0.009) is the same as that of the yellow curve shown in Fig. 6. The frequency of the main disturbance signal is centered near the carrier frequency, and the amplitude of the disturbance signal is amplified as the beam current increases. The amplitude of additional disturbance signals, which are considered to arise from the transient beam loading effect and digital aliasing, also increases with increasing beam current (Color online)

3.3 Disturbance sources in the SRF system

The disturbance signal in the SRF system can be acquired from the measurement system without internal disturbance generation. The frequency of the main SRF system disturbance is centered near the carrier frequency when there is no beam in the ring. The spectra of the disturbance signal under various control conditions without the beam are shown in Fig. 6.

The disturbances from the beam primarily arise from the transient beam loading effect. The spectra of the disturbance signal with the beam are shown in Fig. 7.

The disturbance signals arising from the transient beam loading effect [20–23] and digital aliasing [24] are significant, and the feedback loop has nearly no suppression effect on these signals. It is obvious that the disturbance spectrum near the baseband is worse as the beam current increases. This is because the incident power increases during beam injection and the final power at high beam current is much greater than that at the initial stage [25–27].

4 Conclusion

A digital transfer function measurement system has been embedded into the LLRF system of the SSRF storage ring. The SRF system parameters can be regulated with the open-loop measurement results. The closed-loop measurement results show that the choice of parameters and operation status can drastically affect the transfer function, which determines the stability and control performance of the feedback system. Interaction between cavities through the beam is not negligible, and the system performance is determined by the behavior of all three RF stations. Ripples from the HVPS, the transient beam loading effect, and digital aliasing are the main three disturbance sources for the SRF system. This measurement system will provide experimental verification for model analysis methods and will also define the performance requirements for various new algorithm designs.

References

1. Z.B. Tang, Z.Y. Ma, H.T. Hou et al., Frequency control and pretuning of a large aperture 500 MHz 5-cell superconducting RF cavity. Nucl. Sci. Tech. **25**, 030102 (2014). https://doi.org/10.13538/j.1001-8042/nst.25.030102
2. Z.Y. Ma, J.F. Liu, H.T. Hou et al., Surface preparation processing for superconducting cavities. Nucl. Sci. Tech. **25**, 060102 (2014). https://doi.org/10.13538/j.1001-8042/nst.25.060102
3. X. Zheng, Y.B. Zhao, H.T. Hou et al., DLLRF and beam trip analysis in the storage ring of SSRF. Paper Presented at the Proceedings of 1st International Particle Accelerator Conference, Kyoto, Japan, 23–28 May 2010
4. D. Boussard, G. Lambert, Reduction of the apparent impedance of wide band accelerating cavities by RF feedback. IEEE Trans. Nucl. Sci. **30**, 2239 (1983). https://doi.org/10.1109/TNS.1983.4332774
5. D. Boussard, Control of cavities with high beam loading. IEEE Trans. Nucl. Sci. **32**, 1852 (1985). https://doi.org/10.1109/TNS.1985.4333745

6. M.G. Minty, R.H. Siemann, Heavy beam loading in storage ring radio frequency system. IEEE Trans. Nucl. Sci. **376**, 301 (1996). https://doi.org/10.1016/0168-9002(96)00180-5
7. P. Krejcik, P. Corredoura, M. Minty et al, RF feedback for beam loading compensation in the SLC Damping. Paper Presented at the Proceedings of the PAC93, 2370 (1993). https://doi.org/10.1109/pac.1993.309325
8. Z.G. Zhang, Y.B. Zhao, K. Xu et al., Digital LLRF controller for SSRF booster RF system upgrade. Nucl. Sci. Tech. **26**, 030106 (2015). https://doi.org/10.13538/j.1001-8042/nst.26.030106
9. Z.G. Zhang, Y.B. Zhao, K. Xu et al., Control of field flatness based on FPGA for multi-cell cavity. Nucl. Tech. **40**, 020101 (2017). https://doi.org/10.11889/j.0253-3219.2017.hjs.40.020101. **(in Chinese)**
10. Z.G. Zhang, Y.B. Zhao, K. Xu et al., A calibration method and experiment research based on I/Q demodulation. Nucl. Tech. **38**, 030102 (2015). https://doi.org/10.11889/j.0253-3219.2015.hjs.38.030102. **(in Chinese)**
11. P.P. Gong, Y.B. Zhao, H.T. Hou et al., Front-end frequency conversion module design for harmonic RF system in SSRF. Nucl. Tech. **42**, 010101 (2019). https://doi.org/10.11889/j.0253-3219.2019.hjs.42.010101. **(in Chinese)**
12. M.D. Li, Y.B. Zhao, X. Zheng et al., Design and implementation of frequency tracking and amplitude-phase feedback in RFQ low level control system. Nucl. Tech. **41**, 060202 (2018). https://doi.org/10.11889/j.0253-3219.2018.hjs.41.060202. **(in Chinese)**
13. F. Pedersen, A novel RF cavity tuning feedback scheme for heavy beam loading. IEEE Trans. Nucl. Sci. **32**, 2138 (1985). https://doi.org/10.1109/TNS.1985.4333841
14. F. Pedersen, Beam loading effects in CERN PS booster. IEEE Trans. Nucl. Sci. **22**, 1906 (1975). https://doi.org/10.1109/TNS.1975.4328024
15. Z.K. Liu, C. Wang, L.H. Chang et al., Modeling the interaction of a heavily beam loaded SRF cavity with its low-level RF feedback loops. Nucl. Instrum. Methods Phys. Res. A **894**, 57 (2018). https://doi.org/10.1016/j.nima.2018.03.046
16. T. Mastorides, C. Rivetta, J.D. Fox et al., Analysis of longitudinal beam dynamics behavior and RF system operative limits at high-beam currents in storage rings. Phys. Rev. Spec. Top. Accel. Beams **11**, 062802 (2008). https://doi.org/10.1103/physrevstab.11.062802
17. Y.B. Zhao, C.K. Yin, T.X. Zhang et al., Digital prototype of LLRF system for SSRF. Chin. Phys. C **32**, 758 (2008)
18. F. Qiu, S. Michizono, T. Miura, Application of disturbance observer-based control in low-level radio-frequency system in a compact energy recovery linac at KEK. Phys. Rev. Accel. Beams **18**, 092801 (2015). https://doi.org/10.1103/PhysRevSTAB.18.092801
19. H. Hassanzadegan, R. Grino, A transient model for RF cavity analysis under beam loading. Nucl. Instrum. Methods Phys. Res. A **615**, 143 (2010). https://doi.org/10.1016/j.nima.2010.01.070
20. R. Huang, Y. He, Z.J. Wang, Analytical solution to the transient beam loading effects of a superconducting cavity. Chin. Phys. C **41**, 107001 (2017). https://doi.org/10.1088/1674-1137/41/10/107001
21. J.M. Byrd, S. De, J. Jacob et al., Transient beam loading effects in harmonic rf systems for light sources. Phys. Rev. Accel. Beams **5**, 092001 (2002). https://doi.org/10.1103/PhysRevSTAB.5.092001
22. S.L. Pei, S.H. Wang, Transient beam loading effects in standing wave cavities of linear accelerator. High Energy Phys. Nucl. Phys. **30**, 454 (2006)
23. N. Yamamoto, T. Takahashi, S. Sakanaka, Reduction and compensation of the transient beam loading effects in a double RF system of synchrotron light sources. Phys. Rev. Accel. Beams **21**, 012001 (2018). https://doi.org/10.1103/PhysRevAccelBeams.21.012001
24. T. Mastorides, C. Rivetta, J.D. Fox et al., RF system models for the CERN Large Hadron Collider with application to longitudinal dynamics. Phys. Rev. Accel. Beams **13**, 201801 (2010). https://doi.org/10.1103/PhysRevSTAB.14.029901
25. P.B. Wilson, Beam Loading in High-Energy Storage Rings, SLAC-PUB-1456 (1974)
26. P.B. Wilson, High Energy Electron Linacs: Applications to Storage Ring RF Systems and Linear colliders, SLAC-PUB-2884 (1991)
27. F. Pedersen, RF Cavity Feedback, CERN/PS 92-59 (1992)